INSTITUTE OF PHYSICS PUBLISHING PLASMA PHYSICS AND CONTROLLED FUSION

Plasma Phys. Control. Fusion **48** (2006) 1077–1092 doi:10.1088/0741-3335/48/8/003

L-mode SOL width scaling in the MAST spherical tokamak

J-W Ahn[1], **G F Counsell and A Kirk**

EURATOM/UKAEA Fusion Association, Culham Science Centre, Abingdon, Oxon, OX14 3DB, UK

E-mail: joonwookahn@wisc.edu

Received 31 October 2005, in final form 7 June 2006
Published 5 July 2006
Online at stacks.iop.org/PPCF/48/1077

Abstract

A new data-set of outboard mid-plane scrape-off layer (SOL) heat flux widths, Δ_h, has been constructed for L-mode plasmas in the MAST spherical tokamak (ST). The scaling with key plasma parameters such as density, toroidal magnetic field, parallel connection length in the SOL and surface heat flux at the separatrix is investigated. An empirical scaling is developed for the Δ_h data-set, which exhibits a strong positive dependence on both the connection length (or edge safety factor) and density and weak or moderate inverse dependences on the surface heat flux and magnetic field, respectively. The empirical scaling is compared with earlier results for a range of tokamaks with conventional geometry, which show weaker dependence on the density and edge safety factor. Importantly, however, the weak negative dependence on the surface heat flux (and thus heating power) is common in both conventional and ST geometries. The experimental data are also used to test a number of dimensionally correct Δ_h scalings developed from theoretical models for perpendicular transport in the SOL coupled with classical transport parallel to the magnetic field. A scaling based on perpendicular transport driven by resistive MHD interchange provides the best fit, although several models are close. A subset of the better fitting theoretical scalings are used to extrapolate for Δ_h in one design for a future burning ST machine and finally to predict the peak heat loading on the outboard divertor target plate.

1. Introduction

The lifetime of plasma facing components, especially those at the divertor targets, will be fundamental in determining the availability and cost effectiveness of a future fusion power

[1] Present address: Department of Physics, 1150 University Ave, University of Wisconsin, Madison, WI 53706, USA.

plant. Even in ITER, the divertor target lifetime will be a significant issue. One important factor in determining this lifetime is the peak heat flux that must be accommodated by the targets for a given power flowing into the scrape-off layer (SOL), P_{SOL}. For steady state conditions (ignoring transient phenomena such as edge localized modes and disruptions) this is governed by the radial heat flux width, Δ_{h}, in the SOL.

In a tokamak, either a limiter or a magnetic separatrix defines the plasma boundary. Inside this boundary, where there are closed magnetic flux surfaces, profiles of density and temperature are determined by local perpendicular transport coefficients. Outside the boundary, in the SOL, the profiles are determined by a competition between parallel and perpendicular transport. It is generally accepted that classical processes govern transport parallel to the magnetic field but, in the perpendicular direction, the dominant mechanisms are not fully understood. In order to make predictions for Δ_{h} in future devices it is therefore necessary either to develop scalings from existing devices in terms of well characterized plasma or engineering parameters or to establish a physical basis for the anomalous perpendicular transport and assume that this extrapolates to larger scales.

Several efforts have been made to develop Δ_{h} scalings for conventional tokamaks using multi-machine [1,2] and single-machine [3,4] databases of SOL parameters, however there are few published scalings for the spherical tokamak (ST). It is likely that the extreme magnetic geometry of the ST (low toroidal field, high triangularity, high normalized plasma pressure, high toroidicity and so on) will have a significant impact on perpendicular transport processes in the SOL. Scalings developed from a well-conditioned database of SOL parameters in ST devices are thus a necessity for reliable predictions to future ST devices. To develop such a database, a dedicated series of L-mode discharges covering a broad range of plasma and engineering parameters were produced in MAST. These data were used to develop scalings for Δ_{h} at the outboard mid-plane and to test analytic models for perpendicular transport in the ST SOL.

In section 2, a simple analytic model for transport in the SOL and scaling of the SOL width with basic plasma parameters is briefly described. In section 3 an empirical scaling for the SOL width in MAST is developed using experimental data from a series of L-mode discharges. Section 4 compares the data with dimensionally correct scalings for the SOL width, derived from a variety of physical models for the perpendicular heat diffusivity, $\chi_{\perp}$. Section 5 compares the ST L-mode scaling with one developed from a conventional tokamak database. Lastly, in section 6, a range of L-mode scalings is used to extrapolate from Δ_{h} in MAST to that in a possible future ST device, operating with a D–T mix and an L-mode edge.

2. Theory of SOL transport

2.1. Analytic SOL model

Simple models for the tokamak SOL are usually based on a balance of classical parallel heat transport and perpendicular diffusion. The models are distinguished by the SOL collisionality, which determines the parallel transport, and the choice of cross-field heat diffusivity, $\chi_{\perp}$ Several models for $\chi_{\perp}$ including Bohm diffusion, have been integrated into SOL models by Itoh and Itoh [5] to develop scalings of the SOL width in terms of key operating parameters, such as q_{95}, P_{SOL} and $\bar{n}_{\mathrm{e}}$. This work was extended by Counsell *et al* [6] to include a greater range of parameters in the scaling and to investigate other models for $\chi_{\perp}$.

The balance between the perpendicular (from the plasma core into the SOL) and parallel (along the SOL flux tube to the divetor target) flow of power can be represented in a simplified SOL geometry for a divertor tokamak, figure 1. Here $\chi_{\parallel}$ and $\chi_{\perp}$ are the parallel and

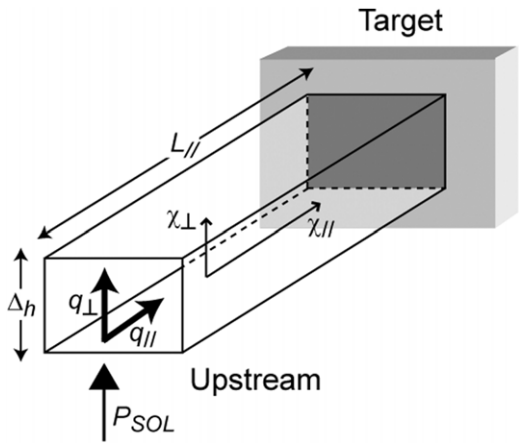

Figure 1. Power balance in a simplified SOL geometry.

perpendicular heat diffusivities, $q_\parallel$ and $q_\perp$ are the heat fluxes, $L_\parallel$ is the upstream to target connection length and Δ_h is the upstream SOL heat flux width. In the case of conduction dominated parallel transport in the SOL, P_SOL, the power crossing the separatrix is given by

$$P_\mathrm{SOL} = A_\perp q_\perp \approx -A_\perp n\chi_\perp \nabla_\perp T = A_\parallel q_\parallel \approx -A_\parallel \kappa_\parallel \nabla_\parallel T \approx -A_\parallel n\chi_\parallel \nabla_\parallel T, \tag{1}$$

where $A_\parallel$ is the area of an annulus at the outboard mid-plane of width Δ_h, projected in the magnetic field direction, and $A_\perp$ is the surface area of the plasma. $\kappa_\parallel$ is the parallel thermal conductivity in the SOL, $\chi_\perp$ is the perpendicular heat diffusivity, n the electron density and T the electron temperature. Making the simplifying assumptions of circular cross-section and large aspect ratio, we then have $A_\parallel = 2\pi(R+a)\Delta_\mathrm{h}\sin\alpha \sim 2\pi R\Delta_\mathrm{h}B_\mathrm{p}/B$ and $A_\perp \sim 2\pi R\cdot 2\pi a = 4\pi^2 Ra$, where α is the field line angle at the outboard mid-plane and B_p and B are the poloidal and total magnetic fields.

Thus, approximating $\nabla_\perp T \sim -T/\Delta_\mathrm{T}$, where Δ_T is a scale-length for perpendicular temperature decay in the SOL, the parallel and perpendicular energy balance equations can be written as

$$n\chi_\parallel \nabla_\parallel T = \frac{B}{B_\mathrm{p}}\frac{P_\mathrm{SOL}}{2\pi R\Delta_\mathrm{h}}, \tag{2}$$

$$n\chi_\perp \frac{T}{\Delta_\mathrm{T}} = \frac{P_\mathrm{SOL}}{4\pi^2 Ra}. \tag{3}$$

Generalized classical heat transfer in the parallel direction can be written as $\chi_\parallel \sim T^\beta \chi_{\parallel 0}$. When $\lambda_\mathrm{ee} \ll L_\parallel$, where λ_ee is the electron–electron mean free path, collisional diffusion becomes dominant in parallel transport, $\beta = 5/2$ and $\chi_{\parallel 0} \sim 1/n$, so that $P_\mathrm{SOL} \propto T^{7/2}/L_\parallel$ (heat loss is limited by the finite conduction in the SOL). On the other hand, if $\lambda_\mathrm{ee} \gg L_\parallel$, the parallel heat flux in the SOL is limited by the transmission of heat through the electrostatic sheath. In collisionless heat streaming, $\beta = 1/2$ and $\chi_{\parallel 0} \sim L_\parallel$, so that $P_\mathrm{SOL} \propto nT^{3/2}$.

It is important to establish a physical basis for the perpendicular heat diffusion, $\chi_\perp$ and its scaling with the plasma parameters. In the model used in this work, following that in [5], temperature and temperature gradient are taken into account. Let $\chi_\perp \sim \chi_{\perp 0}T^\alpha \nabla T^\gamma \sim \chi_{\perp 0}T^\alpha/L^\gamma_{\mathrm{p,T,n}}$ (from micro-turbulence arguments), where $\chi_{\perp 0} \propto n^\delta q^\mu R^\nu a^\sigma B^\lambda$ and L_p, L_T and L_n are the pressure, temperature and density decay lengths in the perpendicular direction.

2.2. SOL width scaling laws

Using the power balance equations, equations (2) and (3), and the expressions for $\chi_{\parallel}$ and $\chi_{\perp}$ described in section 2.1, a scaling of Δ_h with key tokamak parameters (n, q, R, a, B and P_{SOL}) can be obtained. For example, the Bohm model assumes $\chi_{\perp} \sim T/B$ and results in the expression $\Delta_h \propto n^{7/11} R a^{3/11} B^{-7/11} q^{8/11} P^{-3/11}$ for a collisional SOL. Models for turbulence in the SOL have a similar physical basis to those for core turbulence (i.e. ideal and resistive ballooning, interchange modes and drift waves) but with the effects of the limiter or divertor targets included. In this case, the field lines are open and there exists a sheath boundary condition to be imposed at the targets. A detailed description of these theoretical models for SOL width scaling can be found in [6, 7]. One should note that these models can only be adequately validated against data covering a broad parameter regime. In earlier work [5–7], the safety factor at the 95% flux surface, q_{95}, is often used for q. However, for the ST, q_{95} is not necessarily the best measure due to the strong magnetic shear at the edge. In this work, we will therefore compare experimental data with scalings expressed using both q (for which q_{95} is assumed, derived from magnetic equilibrium reconstruction) and parallel connection length in the SOL, $L_{\parallel}$ (calculated from the equilibrium reconstruction by field line following).

3. Empirical SOL width scaling with plasma parameters

3.1. Experimental technique

A dedicated experimental campaign of L-mode plasmas was conducted on MAST to obtain data for the SOL heat flux width, Δ_h, over as wide a range of plasma parameters as possible. Δ_h was determined using data from an array of Langmuir probes across the divertor target strike-point region. Using divertor probes it was possible to derive an accurate Δ_h over a much wider range of discharge conditions than would have been possible using the mid-plane reciprocating probe on MAST. Figure 2 shows a typical MAST magnetic and physical geometry for a connnected double null divertor (CDND) discharge with the probe positions indicated.

An exponential fit to the target heat flux was used to obtain a $1/e$ decay length. This was mapped to the outboard mid-plane, taking account of the flux expansion between the mid-plane and target, using the EFIT magnetic equilibrium reconstruction code [8]. In order to ensure a valid mapping, only data for collisional SOL conditions in the conduction-limited regime were selected (i.e. data where no significant power loss at the target was observed, which might indicate onset of detached conditions). Furthermore, only periods during which the discharges were accurately in a CDND equilibrium were selected, to ensure that complexities in the SOL that might be associated with the existence of a second separatrix were avoided. Thus, data from plasmas for which the outboard δr_{sep} value (the mean radial distance, at the mid-plane, between flux surfaces containing the upper and lower X-points) was greater than 1 mm were discarded (cf a typical ion gyro-radius at the outboard mid-plane, $\rho_i \sim 5$ mm).

The quality of fit obtained in empirical scalings is not only dependent on good conditioning of the data-set but is also crucially dependent on the quality of source data (including accurate estimates of associated errors). Consequently only data from the Langmuir probes with good exponential fits to the electron retardation region and stable ion saturation currents were selected. These data tended to be obtained during quiescent, steady state phases of the discharge which, in any case, are the most appropriate periods to use in the validation of scalings (e.g. because it is most likely that power lost from the core is conducted only to the targets at these times). A typical target heat flux profile for well-fitted Langmuir probe data is shown in figure 3.

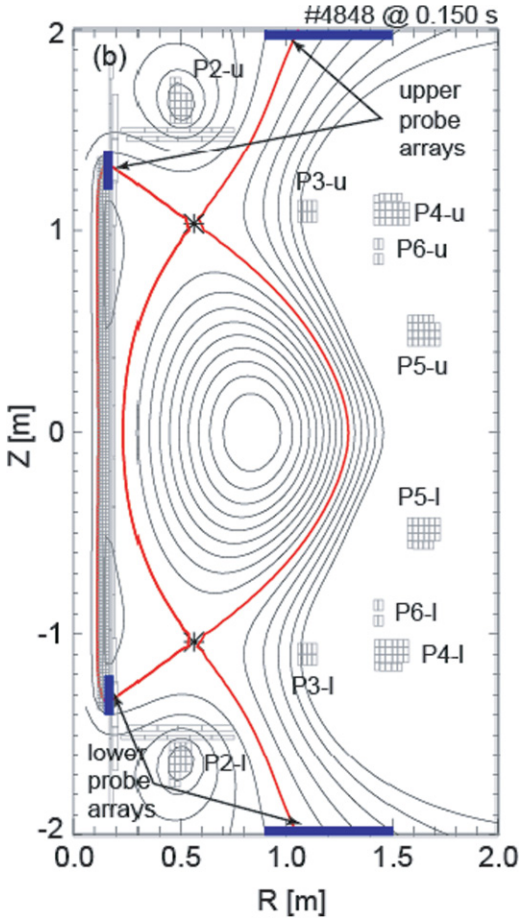

Figure 2. The magnetic and physical geometry of a MAST CDND discharge including positions of the target Langmuir probe arrays. Also shown are the locations of various poloidal coils, both upper and lower.

(This figure is in colour only in the electronic version)

It is seen in figure 3 that the exponential fit is primarily to the steep gradient of the target heat flux profile in the near SOL region (i.e. closer to the separatrix, $1 \leqslant r \leqslant 1.1$ m). This is justified by the fact that only data in the conduction-limited regime, where parallel electron conduction to the divertor dominates heat losses in the near SOL region, were selected for this work. The cross-field heat convection, represented by the flatter profile, is only important in the far SOL region until the divertor detachment sets on [9, 10]. Once the detached conditions set on, the cross-field heat convection to the wall exceeds parallel conduction losses over the entire SOL. This work, therefore, is relevant to the extrapolation to the future machine operating at low/medium density where the divertor detachment is not achieved. The L-mode MAST plasmas operating at line-averaged density below 4.0–4.5 $\times 10^{19}$ m^{-3} generally have electron–ion SOL collisionality of 5–10 and this is consistent with the SOL plasmas in conduction-limited regime.

For each heat flux width derived, four key core plasma parameters were recorded and used to develop an empirical scaling; the line-averaged density, $\bar{n}_e$, power flow across the separatrix

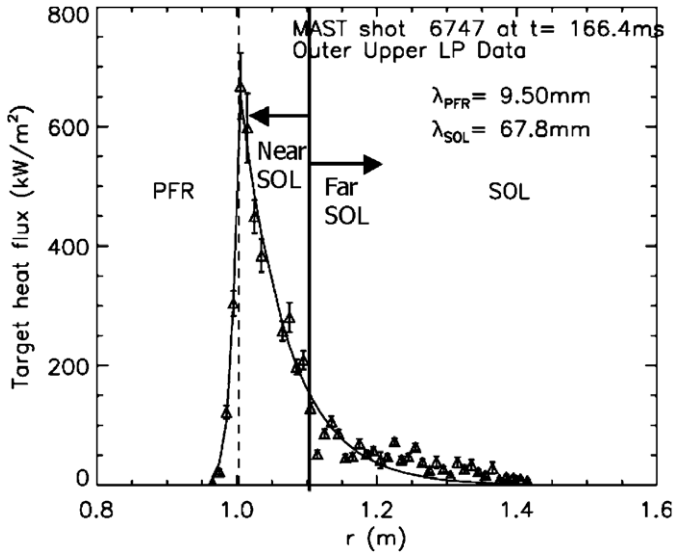

Figure 3. Typical target heat flux profile across the private flux region (PFR) and SOL from target Langmuir probe data. Note that the exponential fitting curve is primarily to the near SOL region.

from the core plasma into the SOL, P_{SOL}, edge safety factor, q_{95}, and toroidal magnetic field at the target, B_{T}. $\bar{n}_{\mathrm{e}}$ was derived from a CO_2 interferometer, P_{SOL} was estimated from the total input power less the radiated power fraction and the rate of change of stored energy and q_{95} and B_{T} from the EFIT code. The range of the plasma parameters explored was $0.28 \leqslant B_{\mathrm{T}} \leqslant 0.41$ T, $0.27 \leqslant P_{\mathrm{SOL}} \leqslant 2$ MW (Ohmic and NBI heated), $4.4 \leqslant q_{95} \leqslant 7.4$ ($10.5 \leqslant L_{\parallel} \leqslant 18.2$ m) and $1.7 \times 10^{19} \leqslant \bar{n}_{\mathrm{e}} \leqslant 4.7 \times 10^{19}$ m^{-3}. Only a very limited range of major and minor plasma radii, R and a, were explored in the plasmas studied (a general difficulty with data-sets derived from a single tokamak). As a result, these parameters were excluded from the empirical scaling.

It is generally accepted that the separatrix density, n_{es}, is directly related to the SOL heat flux width and therefore should be used for the derivation of empirical scalings. The line-averaged density is only permitted for use when density profile consistency over the data-set prevails. However, the mid-plane reciprocating probe data for n_{es} values were not available for construction of the data-set used in this paper. Thus a detailed investigation regarding the justification of the use of $\bar{n}_{\mathrm{e}}$ was carried out by examining relationships between edge n_{e} (e.g. at the 95% or 98% of flux surfaces, $n_{\mathrm{e},95}$ and $n_{\mathrm{e},98}$, respectively) and the scaling parameters for a number of MAST L-mode plasmas, although it could not be conducted for the data points used to derive the empirical scalings (section 3.2) due to the lack of Thomson scattering density profile data at the desired time slices. Figure 4 shows the plot of $n_{\mathrm{e},95}$ versus $\bar{n}_{\mathrm{e}}$ with Spearman's (ρ) correlation coefficient for a wide range of MAST L-mode plasmas. It is clear that the $n_{\mathrm{e},95}$ values are strongly correlated with the line-averaged density values, although with a great deal of scatter. If the scatter were the reflection of the $n_{\mathrm{e},95}$ dependence on B_{T}, q_{95} and P_{SOL} in a systematic way in addition to the relationship to $\bar{n}_{\mathrm{e}}$, then any regression involving $\bar{n}_{\mathrm{e}}$, B_{T}, q_{95} and P_{SOL} alone would automatically be polluted by this interdependence. The relationships of the edge density ($n_{\mathrm{e},95}$ and $n_{\mathrm{e},98}$) to the other parameters (B_{T}, q_{95} and P_{SOL}) have been carefully investigated and found to reveal no systematic interdependences among these parameters within the limits posed by the scatter in the data. The point scatter is therefore not clearly related to any possible interdependence among $n_{\mathrm{e},95}$, $\bar{n}_{\mathrm{e}}$, B_{T}, q_{95} and

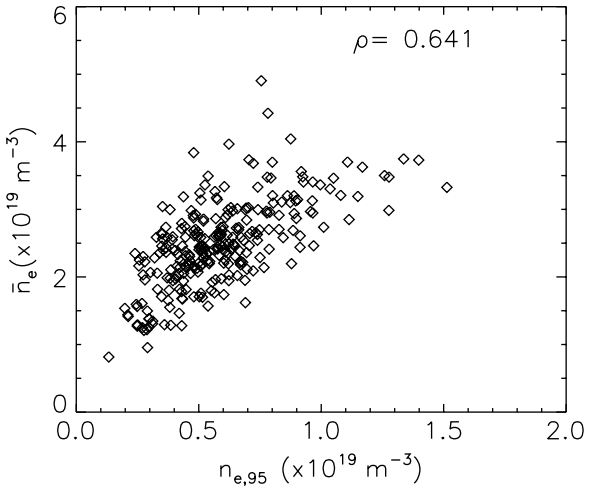

Figure 4. Plot showing strong correlation between the edge density (at 95% of flux surfaces, $n_{e,95}$) and the line-averaged density with Spearman's (ρ) correlation coefficient, for a large number of MAST L-mode plasmas. This, along with the fact that no interdependence between $n_{e,95}$ and other scaling parameters (B_T, q_{95} and P_{SOL}) was identified, indicates justification of the use of $\bar{n}_e$ instead of the separatrix density for the empirical scaling.

P_{SOL}, which however appears to be covered by the noise. The steep edge density gradient in MAST and the moderate spatial resolution (5–8 mm) of the Thomson scattering system at the edge make the extraction of $n_{e,95}$ or $n_{e,98}$ very challenging and this is believed to account for a significant fraction of the scatter.

The use of line-averaged density also allowed a much wider range of discharge conditions in the data-set in that the mid-plane reciprocating probe would only have been able to measure n_{es} for a limited plasma time slice whereas the line-averaged density is continuously measured during the whole plasma discharge time.

It should be noted that there exist co-variances between several of the parameters used in the scaling. For example B_T and q_{95} are implicitly linked and the Ohmic heating power, P_Ω, one component of P_{SOL}, is related to the plasma current, I_p, which affects q_{95} and $L_\parallel$ and so on. Ideally, each parameter should be varied whilst keeping all the others fixed. Such an approach was not, however, possible for this work due, in part, to the wide range over which each parameter was varied. The consequence, as with most empirical scalings, is that the scaling is only strictly valid for extrapolations to devices in which the same co-variances exist.

3.2. Empirical scaling results

A power law regression analysis procedure was employed to investigate the scaling of the outboard mid-plane SOL width. Figure 5 and equation (4) show the result for a scaling of Δ_h in terms of $\bar{n}_e$, B_T, q_{95} and P_{SOL}.

$$\Delta_h(\text{mm}) = 1.16 \times 10^{-28} \bar{n}_e(\text{m}^{-3})^{1.45\pm0.17} B_T(\text{T})^{-0.63\pm0.72} q_{95}^{1.45\pm0.51} P_{SOL}(\text{kW})^{-0.19\pm0.14}. \quad (4)$$

The SOL width has a weak inverse dependence on P_{SOL} ($\propto P_{SOL}^{-0.19}$) and a much stronger positive dependence on both the line-averaged density ($\propto \bar{n}_e^{1.45}$) and q_{95} ($\propto q_{95}^{1.45}$). The apparent strong inverse dependence on the toroidal magnetic field ($B_T^{-0.63}$) cannot be supported due to the large error bars in this case (-0.63 ± 0.72), which are probably a consequence of the relatively

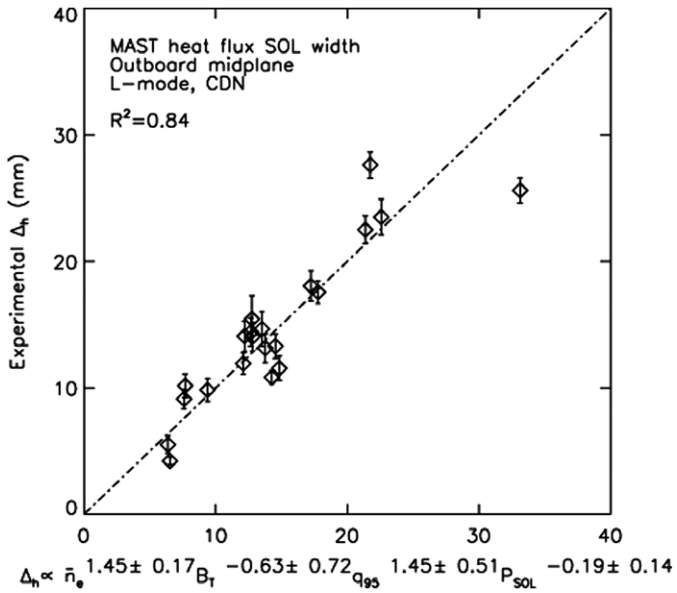

Figure 5. Multivariate least square fit to the MAST database on the outboard Δ_h with respect to $\bar{n}_e$, B_T, q_{95} and P_{SOL}.

small variation of B_T in the database ($0.28 \leqslant B_T \leqslant 0.41$ T). It is noted that the dependence on the line-averaged density and q_{95} is significantly stronger than is observed in conventional tokamak devices (see equation (6)). The size of the current data-set is small (21 points) and this introduces relatively large error bars on the scaling result although the dependences qualitatively agree with the result from conventional tokamaks. The refinement of the scaling and elucidation of possible differences between conventional and ST geometries are subject to an ongoing work. The positive dependence on $\bar{n}_e$ is favourable for extrapolations to future devices, which will operate at higher densities giving rise to a larger Δ_h. This more than offsets the unfavourable, but weak, inverse dependence with P_{SOL}. Extrapolations to future devices will be discussed further in section 6.

We now explore the effect of the ST geometry on empirical scalings in MAST. As the large aspect ratio and circular approximations (especially $L_\parallel \approx \pi R q_{95}$ and $A_\perp \approx 2\pi R \cdot 2\pi a = 4\pi^2 Ra$) used in the derivation of Δ_h are not strictly appropriate in ST geometry, the edge safety factor, q_{95}, and P_{SOL} may not be the most appropriate parameters to choose for the scaling of Δ_h. q_{95} was therefore replaced by the connection length in the SOL from the outboard mid-plane to the divertor target, $L_\parallel$, calculated for each data point using a field-line following code and the EFIT-derived equilibrium. P_{SOL} was replaced by the average heat flux crossing the separatrix, P_{surf}, calculated using P_{SOL} and the plasma surface area derived from the EFIT equilibrium.

Figure 6 and equation (5) present a multivariate least square fit to the MAST SOL width database with respect to $\bar{n}_e$, B_T, $L_\parallel$ and P_{surf}. With this choice of parameters, the scaling now becomes

$$\Delta_h(\text{mm}) = 2.9 \times 10^{-31} \bar{n}_e(\text{m}^{-3})^{1.52\pm0.16} B_T(\text{T})^{-0.98\pm0.69} L_\parallel(\text{m})^{1.69\pm0.48} \times P_{surf}(\text{kWm}^{-2})^{-0.23\pm0.13}. \quad (5)$$

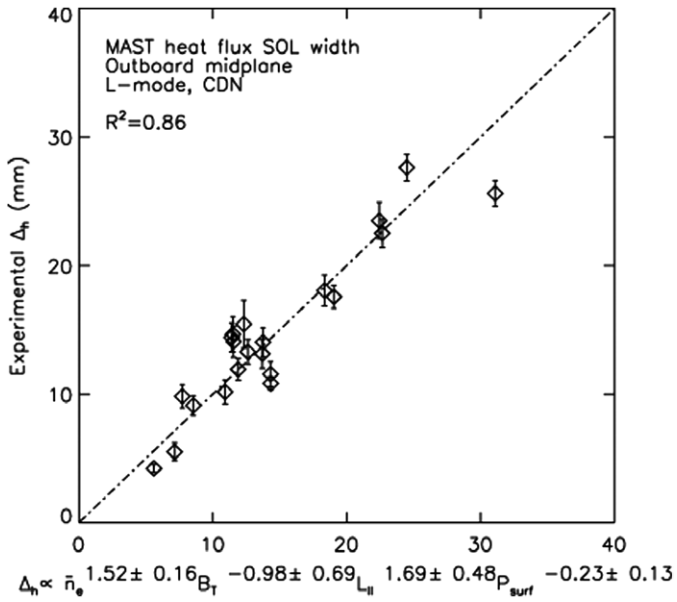

Figure 6. Multivariate least square fit to the MAST database on the outboard Δ_h with respect to $\bar{n}_e$, B_T, $L_\parallel$ and P_{surf}.

Only the index for B_T is noticeably modified by the new choice of scaling parameters, however the change compared with equation (4) (from -0.63 to -0.98) is probably not significant due to the large error bars for the B_T index in both scalings.

The two scaling results, equations (4) and (5), are quite similar and the choice of P_{surf} and $L_\parallel$ does not make a big difference. The large aspect ratio approximation $L_\parallel \approx \pi R q_{95}$ fairly well describes the relationship between $L_\parallel$ and q_{95} for the data points with 5–20% error bars as a whole. The circular approximation $A_\perp \approx 2\pi R \cdot 2\pi a = 4\pi^2 Ra$ also turns out to be quite accurate in estimating perpendicular plasma areas, giving 5–10% error bars for the whole data-set. This produces quite a good linear relationship for P_{SOL} versus P_{surf} and q_{95} versus $L_\parallel$, leading to similar empirical scaling laws (equations (4) and (5)). However, in the future ST machine or even for the plasmas in the planned MAST-U, for which the high elongation and triangularity are likely to be the dominant plasma shaping factors, these approximations will probably become more inaccurate. Therefore the choice of parameter P_{surf} and $L_\parallel$ would be a better representation for the extrapolation to the future ST machine.

4. Comparison with theoretical models for the SOL

Dimensionally correct, heat flux width scalings were derived in [7] from 21 models for $\chi_\perp$, including models based on the effects of resistivity on ballooning and interchange modes, drift turbulence, temperature gradient instabilities and so on. Following the scheme of [7], each $\chi_\perp$ model has been labelled in this work with an index from A to Q. Separate scalings were derived in [7] for collisionless and collisional SOL cases; however, since all the MAST data taken were for SOL conditions in the conduction-limited regime, only the collisional scalings were considered in this study. Five of the $\chi_\perp$ models each gave rise to two separate scalings depending on the choice of perpendicular gradient length. In addition, three directly derived scalings were also considered. Thus a total of 29 collisional scalings were tested against data from MAST.

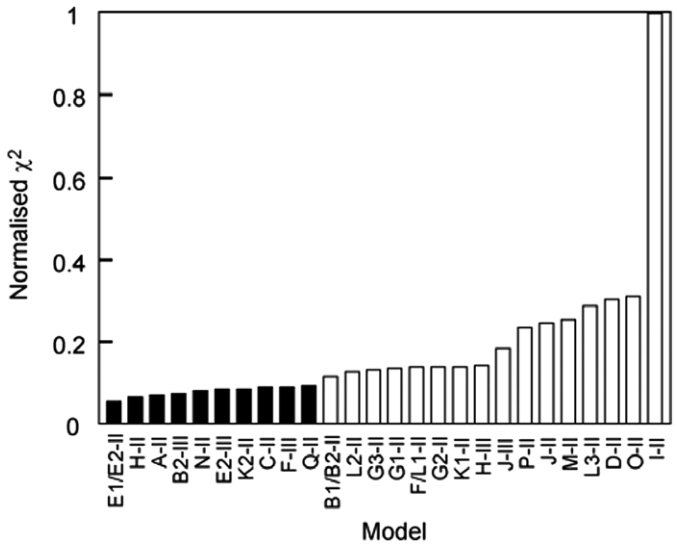

Figure 7. Normalized chi-squared, χ^2, for all the scalings (in order of decreasing quality of fit from the left). The fit was made with respect to the 'ST scaling parameters' (i.e. $\bar{n}_e$, R, B_T, $L_\parallel$ and P_{surf}). The 11 better fitting scalings are shaded black (note that the E1-II and E2-II scalings are indistinguishable).

The original 29 scalings presented in [7] were derived for six parameters: $\bar{n}_e$, R, a, B_T, q_{95} and P_{SOL}. In this study, these have been re-expressed using a maximum of five parameters: $\bar{n}_e$, R, B_T, $L_\parallel$ and P_{surf} in order to take some account of the ST geometry (see section 3.2). Comparisons were made between the value of Δ_h predicted by each of these dimensionally correct scalings and the experimentally measured values. In each case, a chi-squared linear fit was performed. Since the scalings are in the form of a power law, the linear fit was constrained to pass through the origin.

Figure 7 shows the values of chi-squared per degree of freedom (χ^2) for the fit to each scaling. The better fitting models have lower values of χ^2 (re-normalized to 1.0 for the worst model). Eleven of the 29 scalings, shaded black, appear to provide noticeably better fits to the experimental data than the rest (note that the E1-II and E2-II scalings are indistinguishable). Table 1 summarizes the better fitting scalings, together with the associated $\chi_\perp$ model and a brief description of the physics basis for each of the models.

Figure 8 shows scatter plots of the Δ_h derived from the scalings in table 1 against the experimentally measured values. Models E1-II/E2-II, (resistive MHD interchange with L_p and L_n, respectively) produce a least square fit with the lowest χ^2. These two models lead to identical scalings and are thus indistinguishable. The scaling takes the form $\Delta_h \propto \bar{n}_e^{14/15} R^{9/16} B_T^{-14/15} L_\parallel^{16/15} P_{surf}^{-2/5}$ and derives from a model for $D_\perp$ ($\sim \chi_\perp$) based on the resistive MHD interchange mode [7] yielding $\chi_\perp \propto nq^2 R B^{-2} T^{-1/2} L_{p,n}^{-1}$.

The second best scaling, model H-II, has the simpler form $\Delta_h \propto \bar{n}_e^{7/9} B_T^{-7/12} L_\parallel^{5/6} P_{surf}^{-13/36}$, with no dependence on R; this scaling was derived from a model for $D_\perp$ based on drift wave transport [7] yielding $\chi_\perp \propto n^{5/3} q^{10/3} R^{10/3} B^{-2} T^{-11/6} L_n^{-8/3}$.

All the better fitting Δ_h scalings exhibit positive dependences on density, n, and parallel connection length, $L_\parallel$. Dependences on magnetic field, B, (where it appears) are always negative and, in all but one case (model A-II), the dependences on surface heat flux, P_{surf},

Table 1. The 11 better fitting Δ_h scalings for the collisional SOL case, together with the associated $\chi_\perp$ model and a brief description of the physics basis. L_p, L_n and L_T are perpendicular gradient lengths for pressure, density and temperature ($\sim\Delta_{p,T,n} \propto \Delta_h$) contained in some of the theoretical expressions for $\chi_\perp$.

Model	$\chi_\perp$ scaling	Physics basis for $\chi_\perp$	Δ_h scaling
E1-II	$\chi_\perp \propto nq^2RB^{-2}T^{-1/2}L_p^{-1}$	Resistive MHD interchange: with L_p	$\Delta_h \propto n^{14/15}R^{9/16}B^{-14/15}L_\parallel^{16/15}P_{surf}^{-2/5}$
E2-II	$\chi_\perp \propto nq^2RB^{-2}T^{-1/2}L_n^{-1}$	Resistive MHD interchange: with $L_n \sim L_T$	$\Delta_h \propto n^{14/15}R^{9/16}B^{-14/15}L_\parallel^{16/15}P_{surf}^{-2/5}$
H-II	$\chi_\perp \propto n^{5/3}q^{10/3}R^{10/3}B^{-2}T^{-11/6}L_n^{-8/3}$	Drift: with $L_n \sim L_T$	$\Delta_h \propto n^{7/9}B^{-7/12}L_\parallel^{5/6}P_{surf}^{-13/36}$
A-II	—	Marginal ideal MHD	$\Delta_h \propto n^{7/9}R^{11/18}B^{-14/9}L_\parallel^{2}P_{surf}^{2/9}$
B2-III	$\chi_\perp \propto qB^{-2}T^{3/2}L_n^{-1}$	Endplate MHD interchange: with L_n	$\Delta_h \propto n^{21/34}R^{19/33}B^{-14/17}L_\parallel^{33/34}P_{surf}^{-4/17}$
N-II	$\chi_\perp \propto TB^{-1}$	Bohm	$\Delta_h \propto n^{7/11}B^{-7/11}L_\parallel^{8/11}P_{surf}^{-3/11}$
E2-III	$\chi_\perp \propto nq^2RB^{-2}T^{-1/2}L_n^{-1}$	Resistive MHD interchange: with L_n	$\Delta_h \propto n^{35/26}R^{17/31}B^{-14/13}L_\parallel^{31/26}P_{surf}^{-8/13}$
K2-II	$\chi_\perp \propto n^{1/3}q^{2/3}R^{2/3}B^{-2}T^{5/6}L_T^{-4/3}$	Drift Alfven: higher collisionality	$\Delta_h \propto n^{49/78}B^{-28/39}L_\parallel^{51/78}P_{surf}^{-10/39}$
C-II	$\chi_\perp \propto n^1q^3R^1B^{-4}T^{5/2}L_T^{-2}$	Collisionless MHD interchange	$\Delta_h \propto n^{1/2}R^{3/5}B^{-1}L_\parallel^{5/4}$
F-III	$\chi_\perp \propto q^{1/3}R^{1/3}B^{-2}T^{3/2}L_T^{-4/3}$	Drift: with L_n	$\Delta_h \propto n^{5/8}B^{-3/4}L_\parallel^{5/8}P_{surf}^{-1/4}$
Q-II	$\chi_\perp = \text{const}$	Constant $\chi_\perp$	$\Delta_h \propto n^{7/9}L_\parallel^{4/9}P_{surf}^{-5/9}$

(where it appears) are also negative. A dependence on major radius, R, appears in only 6 models (E1/E2-II, A-II, B2-III, E2-III and C-II) and is always positive. The constant $\chi_\perp$ model (which has no physical basis but is often used in fluid models of the edge) provides the simplest form of Δ_h scaling, $\Delta_h \propto \bar{n}_e^{7/9}L_\parallel^{4/9}P_{surf}^{-5/9}$.

Table 2 provides the indices of each scaling parameter for both empirical and 11 better theoretical scalings. The indices of theoretical scalings are represented as decimals instead of fractions for easier comparison with the empirical scaling. It is noted that the $\bar{n}_e$ and $L_\parallel$ dependences of the empirical scaling (1.52 and 1.69, respectively) are particularly stronger than those in most theoretical scalings selected.

5. Comparison with conventional tokamaks

Databases of SOL parameters have been assembled for several conventional tokamaks around the world, partly in response to ITER requirements. Scaling studies of SOL widths have been performed against two different types of experimental measurements: data of the SOL plasma parameters (n_e, T_e, T_i) obtained at the mid-plane using reciprocating probes or spectroscopic diagnostics and data obtained by extrapolating from profiles at the divertor plates, using Langmuir probes or infra-red cameras. Both approaches have been used by the ITER Divertor Modelling and Database Expert Group in order to establish multi-machine databases [1, 2].

Measurements and analysis of the target power deposition by infra-red cameras from four major divertor tokamaks, JET, DIII-D, ASDEX-U and JT60-U, were presented in [2]. All these divertor experiments report that, for Ohmic and L-mode discharges, the SOL width increases with plasma density and edge safety factor and decreases weakly with increasing

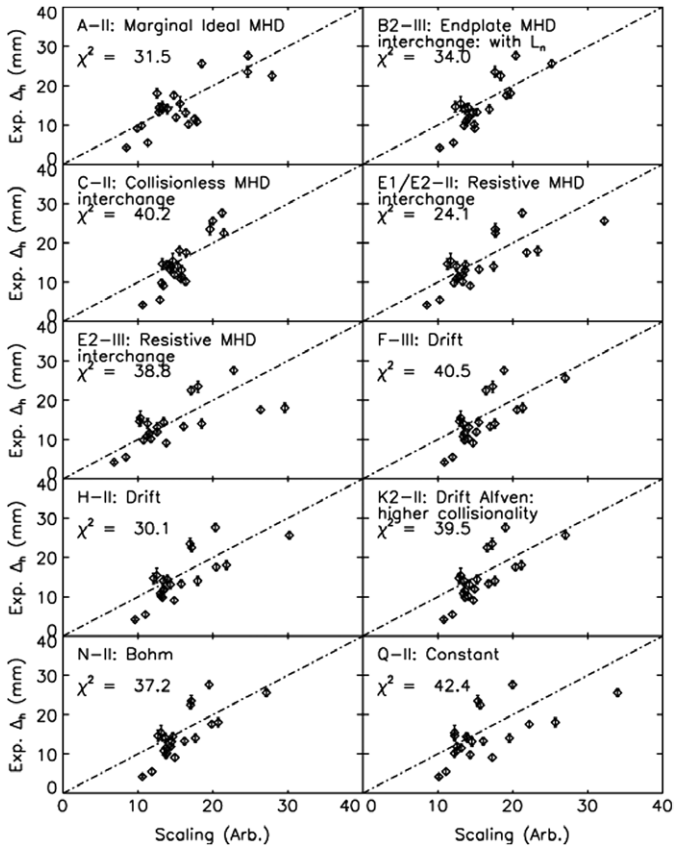

Figure 8. MAST heat flux SOL width data (for the outer SOL in conduction-limited regime) against the 11 best fitting models with respect to the 'ST scaling parameters' (i.e. $\bar{n}_e$, R, B_T, $L_\parallel$ and P_{surf}). Note that the E1-II and E2-II scalings are indistinguishable and are thus plotted on a single graph.

input power—consistent with observations on MAST (see section 3.2). A saturation of the SOL width narrowing with increasing power is, however, observed. The best empirical scaling found within this database for SOL conditions in the conduction-limited regime was reported [2] as

$$\Delta_h \propto \bar{n}_e^{0.68\pm0.16} R^{1.21\pm0.15} q_{95}^{0.59\pm0.11} P_{SOL}^{-0.28\pm0.08}. \quad (6)$$

No dependence on magnetic field was observed.

The scaling shows similar dependences on P_{SOL} to those observed in the MAST empirical scalings (equations (4) and (5)). The dependence on $\bar{n}_e$ and q_{95} (or $L_\parallel$) observed in the MAST data-set are, however, 2 and 2.5 times stronger (respectively) than those in equation (6). In the MAST scaling, the dependence on the toroidal magnetic field at the target is uncertain due to large error bars. It is not, however, inconsistent with the lack of dependance observed in equation (6). The dependence on R could not be investigated in MAST because of the limited variation of R in the data-set.

Table 2. Indices of scaling parameters of the empirical and theoretical Δ_h scalings.

	$\bar{n}_e$	R	B_T	$L_\parallel$	P_{surf}
Empirical fit	1.52	—	−0.98	1.69	−0.23
E1/E2-II	0.93	0.56	−0.93	1.07	−0.40
H-II	0.78	—	−0.58	0.83	−0.36
A-II	0.78	0.61	−1.56	2.00	0.22
B2-III	0.62	0.58	−0.82	0.97	−0.24
N-II	0.64	—	−0.64	0.73	−0.27
E2-III	1.35	0.55	−1.08	1.19	−0.62
K2-II	0.63	—	−0.72	0.65	−0.26
C-II	0.5	0.60	−1.00	1.25	—
F-III	0.625	—	−0.75	0.625	−0.2
Q-II	0.78	—	—	0.44	−0.56

6. Extrapolations to a future ST device

6.1. Model selection

The MAST SOL width data-set is so far quite small (at least for the plasmas optimized for this study), which results in rather large error bars on indices for the empirically-derived Δ_h scalings (equations (4) and (5)). A more comprehensive collection of data on Δ_h, covering a wider range of SOL and core plasma parameters, will be necessary to improve confidence in the empirical scalings before they can sensibly be used to extrapolate for Δ_h in a burning ST device. It is, however, possible to use this data-set to provide a reasonable basis on which to select the theoretical-derived scalings (as presented in table 1) most likely to be valid for a future device.

As we saw in section 4, none of the theoretical scalings examined agree with the empirical scalings within the errors on the indices. We therefore introduce a new criterion for selecting models to be used in the extrapolation. In addition to the filtering procedure based on the quality of fit, χ^2, as described in section 4, we have selected models where the indices agree with those of the empirical scaling (in this case, equation (5)) to within three standard deviations for each index. This method enabled 3 (A-II, C-II and B2-III) out of the 11 models in table 1 to be eliminated as being inconsistent with the experimental data despite their relatively low χ^2. The remaining eight models were used for the extrapolation of Δ_h in a burning ST machine.

6.2. Extrapolation results

The experimental data collected from MAST for these studies are for collisional SOL conditions in L-mode (see section 3.1). It is reasonable to assume that the SOL plasma in a future burning ST device, such as the Culham spherical tokamak power plant (STPP) design [11, 12], will be collisional due to the high core densities. It is also quite possible, and indeed desirable, that such a device could operate with an L-mode edge, for example if associated with an internal transport barrier (L-mode plasmas with confinement comparable to H-mode, $H_{IPB98y,2} > 1.3$, have been observed in MAST [13]). A machine operating in the H-mode may also have L-mode edge plasmas resting on a limiter during start-up. The basic engineering parameters of the STPP relevant to estimating the target heat flux, as well as specific parameters for the SOL scaling, are given in table 3. The parameters of MAST are also given to be compared with STPP so that the extent of the extrapolation is shown.

Table 3. Typical base line parameters together with specific parameters relevant to SOL scaling for a 3 GW STPP. Also presented are the relevant parameters of MAST in order to show the extent of the extrapolation to STPP.

Parameters	STPP	MAST
R, a (m)	3.42, 2.44	0.85, 0.65
P_{fusion}, P_α (MW)	3100, 616	—
P_{aux} (MW)	60	5
B_{T}(T)	1.3	0.5
q_{95}	15	7
$\bar{n}_{\text{e}}(\times 10^{20}\text{m}^{-3})$	1.08	0.35
P_{SOL} (MW)	338	2
Radius at outer target: R_{target} (m)	3	1.15
Outboard separatrix surface area: $A_\perp$ (m^2)	490	18
Outboard parallel connection length: $L_\parallel$ (m)	50	15
Outboard poloidal flux expansion: f	3.5	5
Outboard target inclination: α (°)	10.0	12.0

Table 4. Extrapolation of simple zero-dimensional scalings for the STPP outboard mid-plane SOL heat flux width, for the best fitting 8 models in the order of decreasing quality of fit, together with the average of the models.

Models	E1/E2-II	H-II	N-II	E2-III	K2-II	F-III	Q-II	Average
$\Delta_{\text{h}}^{\text{outer}}$ (mm)	44.2	22.3	19.2	40.6	16.3	15.1	18.2	25 ± 12

The STPP is designed to operate with a double-null divertor configuration (DND). It has previously been reported [14] that ∼95% of core heat losses flow across the outboard separatrix in MAST DND, L-mode plasmas. This assumption, together with the assumption of a 50% radiated power fraction from the core and boundary plasma, was made to estimate P_{SOL} in the STPP. The result is that only 338 MW of the α and auxiliary heating power remains to be handled by the STPP divertor in L-mode: ∼160 MW to each of the outboard legs and ∼8 MW to each of the inboard legs.

The 8 theoretical scalings selected from the 11 listed in table 1 (see section 6) have been used to extrapolate from the mid-plane heat flux width in MAST to the STPP. The results are presented in table 4. Note that the E1-II and E2-II models give identical scalings and thus the same value of extrapolated Δ_{h}.

The extrapolated mid-plane SOL width values range from 15.1 to 44.2 mm. For comparison, the multi-machine empirical scaling developed from a conventional tokamak data-set, equation (6), would indicate a value of 16.3 mm.

We use the average value of Δ_{h} over the eight theoretical scalings, together with the standard deviation, to estimate the target heat fluxes. The predicted outer mid-plane SOL width was used to calculate the parallel mid-plane heat flux, $q_\parallel = P_{\text{SOL}}^{\text{outer}}/2\pi R^{\text{outer}}\Delta_{\text{h}}$, where $P_{\text{SOL}}^{\text{outer}}$ and R^{outer} represent power into the outboard SOL and plasma radius at the outboard mid-plane, respectively. $q_\parallel$ may then be used to derive the peak heat flux at the target, q_{target}, by accounting for the poloidal flux expansion in the outboard SOL, f, the poloidal angle of the target with respect to the magnetic field, α, and the change in radius from the outboard mid-plane to the target, $R_{\text{outer}}/R_{\text{target}}$, using $q_{\text{target}} = q_u F$, where the power reduction factor, $F = \frac{1}{2}(R_{\text{outer}}/R_{\text{target}})\sin\alpha/f$; the factor $\frac{1}{2}$ is from the assumption that power can be evenly divided between the upper and lower targets in a DND configuration. We obtain $F \sim 0.048$ ($\alpha = 10°$, $f = 3.5$ and $R_{\text{outer}}/R_{\text{target}} = (3.4 + 2.4)/3.0$) for the STPP device. The results are summarized in table 5.

Table 5. Outboard mid-plane heat flux SOL width and peak heat flux at the mid-plane and outboard target in L-mode, extrapolated from the average Δ_h given in table 4, for the STPP.

	STPP
Δ_h (mm)	25 ± 12
$q_\parallel$ (MW m^{-2})	348 ± 165
q_{target} (MW m^{-2})	16.9 ± 8

The mean outboard target heat flux, q_{target}, in table 5 of $\sim$17 MW m^{-2} is higher than the levels encountered in existing devices and exceeds even those predicted for ITER but is within the demonstrated power handling capability of high heat flux components already developed for ITER, which are capable of handling steady state heat fluxes of $\sim$20 MW m^{-2}. However, the range of q_{target} that can be derived for the models highlighted in table 3 is large, from a minimum of $\sim$9 MW m^{-2} (in fact, for the best fitting models, E1/E2-II) to just over 27 MW m^{-2} (for model F-III). It cannot therefore be ruled out that novel power handling techniques may be required, and some exploration of technologies applicable to burning STs is already ongoing [15]. Clearly improvements to the database of ST plasmas will help raise confidence in the extrapolation and narrow this range (e.g. data over a wider parameter range, from different size devices and in other modes of operations, such as H-mode), as will improvements to the theory (e.g. to remove the large aspect ratio assumptions).

This study was restricted to developing scalings for the outboard SOL and no predictions for heat fluxes to the inboard targets of the STPP have been attempted in this paper. The development of an inboard SOL scaling awaits construction of a reliable set of inboard data.

7. Summary and conclusions

An empirical mid-plane SOL heat flux width scaling has been developed for the ST, based on a data-set obtained from the outboard SOL in MAST. For the collisional SOL, this scaling shows significantly stronger dependences on the density and edge safety factor (thus parallel connection length) than is observed in a data-set obtained from a range of conventional tokamaks ($\propto \bar{n}_e^{1.45} q_{95}^{1.45}$ in MAST compared with $\propto \bar{n}_e^{0.68} q_{95}^{0.59}$). The dependence on another key parameter, the power flow into the SOL, is however quite similar ($\propto P_{SOL}^{-0.19}$ in MAST compared with $\propto P_{SOL}^{-0.28}$). But, due to the relatively small size of the current data-set, quantitative refinement of the dependences is subject to an ongoing work.

A range of theoretically derived, dimensionally correct scalings was tested against the MAST data. The scalings, originally developed for large aspect ratio conventional devices, were first re-expressed using parameters more appropriate for the ST geometry (specifically edge safety factor and power flow into the SOL were replaced with SOL parallel connection length and surface heat flux at the separatrix). Of the 29 theoretical scalings examined, one based on perpendicular transport driven by resistive MHD interchange provided the 'best-fit', although up to nine other scalings had a similar χ^2. These scalings were used to extrapolate for the heat flux width in a future ST power plant based on the Culham STPP design. The theoretical scalings were used in preference to the empirical scaling as the error bars on the dependences are rather large, reflecting the relatively modest data-set so far constructed. Nevertheless, the empirical scaling was used to eliminate theoretical scalings which were inconsistent with the experimental data (i.e. for which the individual dependences fell outside three standard deviations of the empirical value), reducing the set of scalings studied from 11 to 8. The

average extrapolated heat flux width of 25 ± 12 mm was used to derive the peak heat flux to the outboard target in the STPP, which was calculated as $\sim 17 \pm 8\,\mathrm{MW\,m^{-2}}$.

Acknowledgments

This work was funded jointly by the United Kingdom Engineering and Physical Sciences Research Council and by the European Communities under the contract of Association between EURATOM and UKAEA. The views and opinions expressed herein do not necessarily reflect those of the European Commission. The authors would like to thank Dr K McClements for calculating the geometric SOL parameters for the STPP and Dr J W Connor, Dr H R Wilson and G Voss for many helpful discussions.

References

[1] McCormick K *et al* 1999 *J. Nucl. Mater.* **266–269** 99
[2] Loarte A *et al* 1999 *J. Nucl. Mater.* **266–269** 587
[3] McCormick K *et al* 1992 *J. Nucl. Mater.* **196–198** 264
[4] Itami K *et al* 1992 *J. Nucl. Mater.* **196–198** 755
[5] Itoh S-I and Itoh K 1994 *Plasma Phys. Control. Fusion* **36** 1845
[6] Counsell G F *et al* 1999 *J. Nucl. Mater.* **266–269** 91
[7] Connor J W *et al* 1999 *Nucl. Fusion* **39** 169
[8] Lao L L *et al* 1985 *Nucl. Fusion* **25** 1611
[9] LaBombard B *et al* 2002 *Proc. 19th IAEA Fusion Energy Conf. (Lyon, France)* EX/D2-1
[10] LaBombard B and Lipschultz B 2003 *Plasma Sci. Fusion Center Report* RR-03-8
[11] Wilson H R *et al* 2004 *Nucl. Fusion* **44** 917
[12] Voss G *et al* 2000 *Fusion Eng. Des.* **51** 309
[13] Counsell G F *et al* 2002 *Plasma Phys. Control. Fusion* **44** 827
[14] Counsell G F *et al* 2005 *Nucl. Fusion* **45** S157
[15] Voss G *et al* 2002 *Fusion Eng. Des.* **63** 65